DETERMINATION OF TWO-STROKE ENGINE EXHAUST NOISE BY THE METHOD OF CHARACTERISTICS

A. D. Jones and G. L. Brown

Nelson Industries, Inc.
1981 Acoustical Paper Awards Program
Stoughton, Wisconsin

June 1981

DETERMINATION OF TWO-STROKE ENGINE EXHAUST NOISE BY THE METHOD OF CHARACTERISTICS

A. D. Jones* and G. L. Brown†

University of Adelaide, Adelaide, South Australia

ABSTRACT

A computational technique was developed for the method of characteristics solution of a one-dimensional flow in a duct as applied to the wave action in an engine exhaust system. By using the method it was possible to compute the detailed unsteady flow in both straight pipe and tuned expansion chamber exhaust systems as matched to the flow from the cylinder of a small two-stroke engine. The radiated exhaust noise was then determined by assuming monopole radiation from the tailpipe outlet. Very good agreement with experiment on an operating engine has been achieved in the calculation of both the third-octave radiated noise and the associated pressure cycles at several locations in the different exhaust systems. Of particular interest is the significance of nonlinear behavior which results in wave steepening and shock wave formation. The calculation method developed differs from those of others, principally that of Blair and that of Karnopp, Dwyer and Margolis. The method computes the precise paths on the x-t plane of a finite number of C_+, C_- and P characteristics, thereby obtaining high accuracy in determining the tailpipe outlet velocity and hence radiated noise.

*Presently NRC Research Associate at NASA Langley Research Center, Hampton, Virginia. On leave from Hills Industries, Clarence Gardens, South Australia.

†Presently at California Institute of Technology, Pasadena, California.

1. INTRODUCTION

Until fairly recently, acoustical studies of engine exhaust system elements and the design of muffling devices for internal combustion engines were usually performed using simple linearized acoustic methods based on electrical analogues. Perhaps the most often referenced work in the field is that of Davis et al[1] in which experiments were performed which justified the relatively simplistic approach for the design of a variety of acoustic filters for conditions of zero mean flow and low sound pressure levels. Subsequently, the work of Alfredson and Davies[2,3] advanced the linearized analysis to the stage where a mean gas flow through a variety of muffling devices was considered in the calculation with no loss of accuracy. More recently, Young and Crocker [4,5] devised a calculation technique in which the linear acoustic transmission loss of mufflers with complex shapes was found using a finite element analysis. In their analysis they described the transmission characteristics of muffler elements in terms of four-pole matrices and thus modeled complete mufflers by the cascade connection of the various matrices in analogous transmission lines.

There are, however, serious limitations in the applicability of linear theories, such as the above, as the exhaust noise is a result of wave action in the muffler following the rapid release of gas from an engine cylinder. This wave action results in large amplitude pressure waves, particularly in the upstream regions of the muffler system. A linear theory cannot account for the wave steepening that occurs in large amplitude waves nor can it include the nonlinear behavior of various exhaust system elements, for example, resistances. A further difficulty in application of linear theories is the requirement that the engine exhaust be specified as an acoustic source of some

strength and impedance. Since in a two-stroke engine, for example, the engine will vary from practically a current source as the exhaust port begins to open to almost a voltage source with the port fully open, there can be no simple characterization of its impedance. In addition, linear theory can take no account of variable entropy along the duct, due for example to imperfect scavenging or to standing shocks of varying strength at the exhaust port. This additional complexity is simply handled within a nonlinear model.

To overcome these well-known problems with linear theory and more adequately describe the gas dynamics, the method of characteristics has been applied by Blair and others[6,7,8] to study the generation and nature of exhaust noise for several simple exhaust systems for (usually) small two-stroke engines.

The use of the method of characteristics to study the wave action in engine exhaust systems is by no means new and the method of characteristics has been so used for about 30 years. However, such work has been mainly concerned with engine operation and efficiency and not with radiated exhaust noise. Of this work, perhaps the most well known is that of Benson and his colleagues. Using a particular numerical approach[9], Benson and co-workers have developed codes to calculate various aspects of engine operation for a great many engine and exhaust systems, for example reference 10, but they have not been concerned with radiated noise.

Blair subsequently used Benson's same method to study, initially, performance aspects[11] and, later, radiated engine exhaust noise[7,8] mainly for motorcycle engines. Benson's method, however, is shown below in section 2.8 to be inherently inferior to the method described below, for exhaust noise studies. In essence this is due to the fact that Benson uses a "mesh" method to compute the x - t diagram for the exhaust system, with a limited

number of fixed mesh points along the duct, whereas, the present method computes the precise paths on the x - t plane of a finite number of C_+, C_- and P characteristics. With a sufficient number of mesh points Benson's method may well give adequate accuracy but the present results suggest that following the characteristics directly ensures that "points are placed where they are needed." This approach seems preferable, particularly if the result is an input to an acoustic calculation. This is discussed further in section 2.8.

In other recent studies[12,13,14] finite difference methods have been used to compute the one-dimensional wave motion in single cylinder engine exhaust systems. The works of Lakshminarayanan et al[13] and Walter and Chapman[14] were concerned with aspects of engine operation and performance, however, Kornopp, Dwyer and Margolis[12] have used their analysis to compute radiated exhaust noise. As their method considers fixed points along a one-dimensional duct system (like Benson's) and fixed time intervals, it is expected to be similarly less accurate than the method described below in the prediction of noise, though in this case no direct comparison has been made.

When this present work was commenced it was decided to devise a calculation technique by which the actual wave diagram would be calculated rather than to use an existing calculation method. The approach and the results of the study are described below along with comparisons with experiment and with other numerical approaches.

2. METHOD OF SOLUTION

In essence the problem, firstly, is to match at the engine exhaust port an unsteady one-dimensional gas-dynamics calculation of the flow in the

exhaust duct to the flow out of the cylinder, and then to match an acoustic calculation for the far-field noise to the flow at the outlet of the exhaust duct. The application of the method of characteristics to unsteady, one-dimensional gas-dynamics problems is well-known (for example, Rudinger[15] and Whitham[16]) but the boundary conditions in this problem are not straight forward. Also the computational procedures usually employed (i.e., graphical) are not convenient and new procedures are necessary for the convenient and accurate determination of, specifically, the radiated noise.

A brief discussion of the essential aspects of the method of characteristics as applied in this problem is given in section 2.1 and the specific boundary conditions and computational procedures follow in sections 2.2, 2.3 and 2.4.

2.1 Method of Characteristics

In this model of the duct flow, wall friction and heat conduction to the wall are neglected. This initial simplifying assumption may be corrected subsequently within the framework of the method of characteristics (e.g., Rudinger[15]), however, this has not been considered necessary within the analysis so far.

For a duct of slowly varying area A, the conservation equations in this case are

$$\rho_t + u\,\rho_x + \rho\,u_x = -\rho\,u\,\frac{A_x}{A} \tag{1}$$

$$\rho\,u_t + \rho\,u\,u_x + p_x = 0. \tag{2}$$

$$s_t + u\,s_x = 0 \tag{3}$$

which may be rewritten in characteristic form (Whitham[16]) as

$$\frac{1}{\rho a}\frac{dp}{dt} \pm \frac{du}{dt} = -\frac{auA_x}{A} \quad \text{on } C_+, C_-: \quad \frac{dx}{dt} = u \pm a \tag{4}$$

and $$\frac{ds}{dt} = 0 \qquad \text{on P:} \qquad \frac{dx}{dt} = u. \tag{5}$$

The entropy is then constant on particle paths (P characteristics). In this numerical solution it is assumed that the P characteristics mark entropy discontinuities so that the entropy is constant between P characteristics. Within such a region it follows that, for a perfect gas, $\frac{dp}{dt} = \left(\frac{2}{\gamma-1}\right)\rho a \frac{da}{dt}$. For a region where $A_x = 0$ it then follows from equation (4) that the Riemann variable

$$P_1 = \left(\frac{2}{\gamma-1}\right)\frac{a}{a_0} + \frac{u}{a_0} \tag{6}$$

is constant on C_+ in any region between P characteristics (a_0 is reference speed of sound) and similarly

$$Q_1 = \left(\frac{2}{\gamma-1}\right)\frac{a}{a_0} - \frac{u}{a_0} \tag{7}$$

is constant on C_- in this region. For $A_x \neq 0$ then, if a C_+ (or C_-) characteristic is advanced in x by $\Delta x = (u + a)\Delta t$ (or $(u-a)\Delta t$), we see from equations (4) and (6) that, for s constant,

$$\Delta P_1 (\text{or } \Delta Q_1) = -\frac{auA_x}{a_0 A}\Delta t. \tag{8}$$

Thus, in general, the problem of finding the flow in the duct is reduced to plotting the paths of C_+, C_- and P characteristics on an x-t diagram, keeping track of the Riemann variable on C_+ or C_- and the entropy on P characteristics. The Riemann variable will change due to changes in area as in equation (8) or due to intersections of the C_+ or C_- with P characteristics

at which points there may be discontinuous changes in entropy. The change in P_1 or Q_1 at such an intersection is obtained in the usual way using the fact that the final pressures and velocities on either side of the entropy discontinuity must be the same. In addition to the intersection of C_+ or C_- with P characteristics, the other events in the x-t diagram that need to be calculated are the intersection of C_+ with C_- and the arrival of C_+, C_- or P characteristics at either the engine exhaust port or the open exhaust outlet (i.e., the end of the tailpipe). It is these latter boundary conditions which require more detailed consideration.

We note in passing that while nonlinearity is expected to play a crucial role in describing the exhaust wave system it was expected that any propagating shocks that did form would not be large enough to produce changes in entropy comparable with the other sources of entropy variation (combustion temperature, incomplete scavenging, standing shocks). The overtaking of a C_+ (or C_-) characteristic may therefore be treated simply as the formation of a weak shock producing no entropy change but with the resultant shock having a velocity which is the mean of the $\frac{dx}{dt}$ for the two intersecting characteristics. (These are the well-known, asymptotic properties of weak shocks.) For simplicity, however, when the x-t diagram was computed, the velocity of the weak shock was approximated to the velocity of the faster characteristic. This approximation had little effect on the calculations described in section 3 as the overtaking of C_+ (or C_-) characteristics was found to be extremely uncommon. (It occurred only twice throughout all these calculations).

Some further approximations for convenience and the way in which the x-t diagram was computed are described in section 2.4.

2.2 Boundary Conditions

The only boundary conditions considered in the analysis are:

1. open exhaust port
2. closed exhaust port
3. open tailpipe

In the x-t diagram, whenever a C_+ or C_- characteristic reaches one of these types of boundaries, a characteristic of opposite type is reflected. If the resultant flow is into the duct through the boundary, a P characteristic is also added.

Case 2 is relatively simple and is described in Rudinger[15]. Case 3 can be considered with various levels of approximation. In this calculation the approximation made is that for outflow the pressure at the plane of the exhaust is p_{ao} (the atmospheric pressure) and constant, while for inflow (when it exists) it is assumed that the isentropic, compressible Bernoulli equation holds (i.e., quasi-steady flow is assumed from p_{ao} into the tailpipe) and the pressure at the tailpipe is therefore less than p_{ao}. The flow at the open exhaust port (case 1) is much more complex, however, as it matches the cylinder conditions to the gas flow in the exhaust pipe. The open exhaust port is clearly the most important boundary in the x-t diagram.

2.2.1 Open exhaust port

When a C_- characteristic reaches the open exhaust port, the resultant flow is either inflow or outflow from the cylinder, which is either choked or unchoked at the port. As mentioned above, there will be a reflection and, if there is outflow, a P characteristic is added. Figure 1 shows a section of an x-t diagram describing the occurrence of outflow in the region near to

the exhaust port. A pictorial representation of the engine and exhaust duct is also shown, with the relative size of the latter exaggerated. It is clear how the P characteristic marks the entropy discontinuity.

It is worth considering this case in some detail as it characterizes the way in which the whole problem has been approached. The code stores for each characteristic its current location, the value of the speed of sound, the fluid velocity, the entropy and the current value of the Riemann variable. Thus, in figure 1 at the time at which the C_- arrives at the exhaust port Q_1, s_d, u_2 and a_2 are known. By keeping track of previous mass flux through the exhaust port and from the crankcase into the cylinder (section 2.3) the conditions in the engine cylinder at this time t are also known (i.e., $p_c(t)$, $a_c(t)$ and from the equation of state $s_c(t)$). This information, along with the current value of the exhaust port area, A(t), is sufficient to decide whether there is inflow or outflow from the cylinder and whether this flow is choked or not. This is considered later in section 2.2.2. Assuming outflow, for the present, when a C_- reaches the port, in addition to a reflected C_+ a P characteristic is required to satisfy these boundary conditions. The unknowns are then s_4, u_3, a_4, p_d, a_3. (P_1 for the C_+ is found from u_3 and a_3 using equation (6).) These variables are found from the following equations. Quasi-steady, adiabatic flow through the exhaust port is assumed so that

$$a_4^2 + \left(\frac{\gamma-1}{2}\right) u_3^2 = a_c^2(t) \tag{9}$$

From the Riemann variable for C_- we have

$$Q_1 = \left(\frac{2}{\gamma-1}\right) \frac{a_2}{a_o} - \frac{u_2}{a_o} = \left(\frac{2}{\gamma-1}\right) \frac{a_3}{a_o} - \frac{u_3}{a_o} \tag{10}$$

(Note: For a slowly varying area duct, the values of u_2 and a_2 held in the code will refer to the previous time the C_- had its Riemann variable changed, and so will not relate to the updated value Q_1, however, this will not at all affect the application of equation (10) as u_3 and a_3 will so relate to Q_1 in any case.)

Assuming the exhaust is a perfect gas whose entropy is given by

$$\frac{s-s_o}{R} = \ln\left[\left(\frac{a}{a_o}\right)^{\frac{2\gamma}{\gamma-1}} \cdot \frac{p_o}{p}\right] \tag{11}$$

where p_o, s_o, a_o = reference conditions, then since $p_d = p_3$ we have

$$\frac{a_4}{a_3} = e^{\left(\frac{\gamma-1}{2\gamma R}\right)(s_4-s_d)} \tag{12}$$

Similarly, the conditions in the cylinder and those in region 4 are related by

$$\frac{s_4-s_c(t)}{R} = \ln\left[\left(\frac{a_4}{a_c(t)}\right)^{\frac{2\gamma}{\gamma-1}} \cdot \frac{p_c(t)}{p_d}\right] \tag{13}$$

and the mass flux through the port can be expressed in the form

$$C(t)\, \rho_c(t)\, a_c(t)\, A(t) = \rho_4 A_d u_3$$

or

$$C(t)\, \frac{p_c(t)A(t)}{a_c(t)} = \frac{p_d\, A_d\, u_3}{a_4^2} \tag{14}$$

The five equations (9), (10), (12), (13), (14) and an additional equation for the flow parameter $C(t)$ are sufficient to solve for the five unknowns above.

For choked flow the mass flux depends only on the stagnation conditions in the cylinder and $C(t)$ in equation (14) is given by the familiar result for isentropic flow up to a sonic throat

$$C(t) = \left(\frac{}{\gamma+1}\right)^{\frac{\gamma+1}{2(\gamma-1)}} \qquad (15)$$

For subsonic flow, isentropic flow is assumed up to the minimum area. The pressure at this point can now be assumed to be uniform across the whole duct area and this pressure related to p_d by the conservation of momentum. For a small port area the pressure recovery is negligible, the pressure at the port is approximately p_d and $C(t)$ is found to be

$$C(t) = \left(\frac{2}{\gamma-1}\right)^{1/2} \left(\frac{p_c(t)}{p_d}\right)^{-\frac{(\gamma+1)}{2\gamma}} \left[\left(\frac{p_c(t)}{p_d}\right)^{\frac{\gamma-1}{\gamma}} - 1\right]^{1/2} \qquad (16)$$

This is an adequate approximation in the present context so that all the quantities required for the continuation of the x-t diagram may now be found. A similar approach is followed for inflow from the duct to the cylinder, where choked flow is also a conceivable possibility.

2.2.2 Type of exhaust port flow

Continuing from the above analysis, the criterion for the existence of either inflow or outflow from the cylinder may easily be found. To determine this, the equations (9), (10), (12), (13) and (14) may be applied to outflow from the cylinder for which $u_3 \to 0$. From equation (9), it follows that $a_4 = a_c(t)$, for this flow. Also, equation (10) becomes

$$Q_1 = \left(\frac{2}{\gamma-1}\right) \frac{a_3}{a_o}$$

Hence, $a_3 = a_o\left(\frac{\gamma-1}{2}\right) Q_1$. For zero flow $p_c(t)$ must equal p_d, hence, from equation (13) as $a_4 = a_c(t)$ we see that $s_4 = s_c(t)$. Then, by substituting

for a_3, a_4 and s_4 in equation (12) and by then substituting for $a_c(t)$ in terms of $p_c(t)$, $s_c(t)$ and the reference conditions, using a form of equation (11), it follows that for the final flow velocity to be zero after a C_- reaches the port, the value of the Riemann variable Q_1 for the C_- is

$$Q_1 = \left(\frac{2}{\gamma-1}\right) \left[\frac{p_c(t)}{p_o}\right]^{\left(\frac{\gamma-1}{2\gamma}\right)} e^{\left(\frac{\gamma-1}{2\gamma R}\right)(s_d-s_o)} \tag{17}$$

If the value of the Riemann variable of the incident C_- is greater than that given by equation (17), inflow to the cylinder will occur (because this corresponds with a higher pressure in the duct than in the cylinder) and if less, outflow.

The existence of either choked or subsonic flow may similarly be determined by a test on the value of the Riemann variable Q_1 for the incident C_-. For outflow, again equations (9), (10), (12), (13), (14) are used. In this case, a flow which is barely sonic in the exhaust port is considered, as discussed below.

For sonic flow in the exhaust port, as the flow is isentropic from the cylinder, there is a fixed relation between the reservoir pressure $p_c(t)$ and the throat static pressure. Then, for a subsonic flow which is barely sonic in the port, as the throat static pressure is assumed equal to p_d, as mentioned above, it follows that

$$p_d = p_c(t) \left(\frac{2}{\gamma+1}\right)^{\frac{\gamma}{\gamma-1}} \tag{18}$$

By now substituting for p_d using equation (18) and for C(t) for choked flow from equation (15) in equation (14) we get

for barely sonic outflow $$\frac{A(t)}{a_c(t)} \cdot \left(\frac{\gamma+1}{2}\right)^{1/2} = \frac{A_d\, u_3}{a_4^2} \qquad (19)$$

The conditions to cause barely sonic outflow may now be obtained simply from equations (9) and (19) as these have only u_3 and a_4 as unknowns. Hence, the value of the Riemann variable Q_1 for a C_- which results in outflow from the cylinder which is choked in the exhaust port is

for choked outflow $$Q_1 < \left(\frac{2}{\gamma-1}\right)\frac{a_c(t)}{a_o}\left(\frac{2}{\gamma+1}\right)^{1/2} e^{\left(\frac{\gamma-1}{2\gamma R}\right)(s_d - s_c(t))}$$

$$\cdot \left[-\frac{a_c(t)}{a_o}\left[\left(\frac{2}{\gamma-1}\right) + \left(\frac{2}{\gamma+1}\right)\left(\frac{1}{\gamma-1}\right)^2\left(\frac{A_d}{A(t)}\right)^2\right]^{1/2} + \frac{a_c(t)}{a_o}\left(\frac{2}{\gamma+1}\right)\left(\frac{1}{\gamma-1}\right)^2\left(\frac{A_d}{A(t)}\right)^2\right]^{1/2} \qquad (20)$$

The expression for choked inflow is similarly found.

2.3 Cylinder and Crankcase Conditions

In the process of computing the x-t diagram, the cylinder and crankcase conditions are updated every time a C_- characteristic reaches the open exhaust port. It is assumed that a steady flow has existed since the previous C_- characteristic reached the port. First, the mass exchange between the cylinder and exhaust pipe, over the whole time period involved, is considered separately. New cylinder conditions are obtained. Then, using these cylinder conditions together with the unchanged crankcase conditions, the mass exchange between the two volumes is determined and new conditions in each are obtained. (For simplicity the transfer port length is taken as zero). Immediately after the

new cylinder and crankcase conditions are determined, the calculations for the reflection of the current C_- characteristic are performed.

The mass transfer calculations are noteworthy as they are performed in terms of a variable $\lambda(t)$ which represents the reciprocal of a characteristic time to exhaust the cylinder. In this way the values of pressure, temperature, etc. of the mass remaining in the cylinder are obtained as a function of the rate of port opening. This is explained briefly below.

The mass flow rate out of the cylinder may be expressed in terms of the cylinder conditions, the exhaust port throat area and the flow parameter $C(t)$. The parameter $C(t)$ is constant for choked flow and for subsonic flow is related to the pressure ratio between the reservoir (cylinder) and the throat static pressure (equal to static pressure just downstream of the port, as explained in section 2.2.1).

Thus,
$$\dot{m}(t) = C(t)\, \rho_c(t) a_c(t) A(t) \tag{21}$$

where $\dot{m}(t)$ = mass flow rate as a function of time.

If
$$\lambda(t) = \frac{C(t) a_c(t) A(t)}{V_c(t)} \tag{22}$$

where $V_c(t)$ = volume of cylinder, then

$$\dot{m}(t) = \lambda(t)\, M_c(t) \tag{23}$$

where $M_c(t)$ = total mass in cylinder. It may then be shown that

$$\dot{m}(t) = \lambda(t)\, M_c(0)\ e^{-\int_0^t \lambda\,(t)\, d(t)} \tag{24}$$

where $t = 0$ at the time of E.P.O. (exhaust port opening).

This is the required general solution for the mass flow rate $\dot{m}(t)$. The properties of the gas in the cylinder may now also be expressed in terms of $\lambda(t)$ and various initial conditions. For example, the pressure may be expressed as

$$p_c(t) = p_c(0) \left|\frac{V_c(0)}{V_c(t)}\right|^{\gamma} e^{-\gamma\int_0^t \lambda(t)dt} e^{-(\gamma-1)(s_c(0)-s_c(t))/R} \qquad (25)$$

Therefore, to obtain the cylinder conditions, the integral of $\lambda(t)$ is progressively obtained numerically. As well as the $\lambda(t)$ integral for the cylinder, there is a separate similar integrating calculation performed for the crankcase in terms of a variable, $\lambda_{cr}(t)$. In the case of flow between the crankcase and cylinder there is, of course, an entropy change in the lower pressure volume. It is found, for example, that the entropy change in the cylinder, as a result of a flow from the crankcase, is given in terms of $\lambda(t)$ and the pressures and temperatures in both volumes.

2.4 Computation Method

Essentially, the computation method used numerically plots the precise paths of a finite number of C_+, C_- and P characteristics on an x-t diagram. The means of doing this has been arranged to suit the kind of output information that has been required. Specifically, the pressure cycle at certain points in the exhaust pipe and the velocity cycle at the tailpipe outlet were required.

The calculation for the x-t diagram starts with an even distribution of C_+ and C_- characteristics in the duct at time $t = 0$. Typically a total of 60 C_+ and C_- characteristics is often used. The initial particle velocity throughout the pipe is zero, the pressure being atmospheric and the entropy

value throughout the duct is usually set equal to that in the cylinder when the exhaust port opens. This is done as this entropy value turns out to be a rough average of the resultant entropy levels of the exhaust gas in the duct. The initial cylinder conditions are based on actual measured pressure values at exhaust port opening, and estimated temperature values. The initial crankcase conditions are based on the assumption of atmospheric pressure and temperature in the crankcase at the time of the inlet port closing.

At regular small intervals of time Δt, typically 10^{-6} seconds, the characteristics are moved to new positions along the duct. When events such as characteristics crossing or a characteristic reaching a duct boundary occur, the correct final flow situation is put in the characteristic diagram. When a C_+ characteristic reaches the open tailpipe, the new calculated value of outlet velocity is stored in an array together with the value of time after E.P.O. This obviously very fine resolution of the tailpipe outlet velocity is significant in the accurate calculation of the radiated sound pressure cycle, as shown in section 2.6 below.

When the pressure values at any point in the duct are calculated they are obtained from the x-t diagram at regular large intervals, typically 100 Δt or 10^{-4} seconds. They are, in fact, obtained by interpolating between the values behind the nearest characteristics. This resolution of the pressure is, of course, not as fine as that of the velocity, but greater resolution has not been necessary.

Several approximations are made which assist in the computation without significantly affecting the accuracy.

First, whenever a C_+ (or C_-) characteristic meets a P characteristic, although the final C_+ (or C_-) and P characteristics are correctly described

in the calculation, the C_- (or C_+) characteristic reflection is not added to the x-t diagram. It may be simply shown that this is a correct procedure as none of the C_+ and C_- characteristics in the whole x-t diagram is given an incorrect Riemann invariant as a result. The second approximation is concerned with a subroutine which is used to limit the number of total P characteristics present by periodically merging together some adjacent P characteristics which have no intermediate C_+ or C_- characteristics. It may be shown that if this is done so that mass is conserved, then momentum and energy are also conserved and there is a slight increase in entropy. Clearly, these approximations both involve a negligible loss of accuracy. This was checked by performing test calculations for which there are known solutions for simple finite waves.

Further approximations are made in regard to the analysis of a duct with slowly varying area. Firstly, the Riemann variable for a C_+ (or C_-) characteristic is updated to allow for changes in cross section only just before the C_+ (or C_-) is about to meet either another characteristic or a duct boundary. Also, in application of equation (8) it is assumed that the flow values, a and u, associated with a particular C_+ (or C_-) have not changed since the previous event in the x-t diagram the characteristic was involved in. Therefore, these values of a and u are used to determine ΔP_1 (or ΔQ_1) together with the elapsed time between events Δt and a value of A_x/A obtained from the known geometry.

Calculations of a conical segment of a spherical implosion for which there is an exact solution, discussed in section 2.7, and the calculations for a tuned expansion chamber, discussed in section 3.3 show that these above-mentioned approximations are entirely adequate. In the calculations for a

tuned expansion chamber, with 60 initial C_+ and C_- characteristics, occasionally the characteristics became sparsely separated in some of the five different segments of the exhaust system, however, the computation method functioned adequately with as few as three characteristics in a segment with a 20 times area change.

As well as the above-mentioned simplifications, the omission from the analysis, so far, of heat loss through the duct walls and also viscous losses is quite reasonable, as shown by the good agreement with experiment detailed in section 3.

2.5 Sample Calculations for Straight Exhaust Pipes

It is useful to now consider sample calculations made using the method described in the preceding sections. Firstly, a computed x-t diagram will be studied. This makes the method of computation clearer and shows several interesting features.

2.5.1 Computed x-t diagram

Figure 2 shows a typical computed x-t diagram which simulates about two-thirds of one cycle in a straight pipe exhaust on a single cylinder two-stroke engine. The operating conditions assumed for the calculation are an engine speed of 6000 rpm and a pressure in the cylinder at E.P.O. of 700 kPa absolute. Of course, these values are a considerable exaggeration and were used purely to make the various events stand out. For simplicity, only 12 initial C_+ and C_- characteristics were used and this small number made it possible to leave in the x-t diagram all the P characteristics added at the exhaust port, although for clarity, the paths of only two are shown.

It is clear how the calculation commences with the C_+ and C_- characteristics describing a flow in the duct with uniform entropy and zero velocity. When the first C_- reaches the open exhaust port it is clear that there is a reflected C_+ and an introduced P characteristic. This reflected C_+, of course, represents the initial wavefront on the exhaust pulse. The first few reflected C_+ characteristics are seen to describe the high pressure exhaust pulse as it is clear that they accelerate the gas downstream as shown by the way the C_- characteristics are slowed down by them and by the way they accelerate the first P characteristic. Further, it is clear that the initial exhaust pulse is reflected from the open tailpipe end as an expansion wave of low pressure, as expected. This is shown in the way the converging C_+ characteristics are reflected at the boundary as diverging C_- characteristics, forming an expansion fan and in the way these C_- characteristics accelerate the gas particles, represented by the P characteristics, downstream.

The leading P characteristic represents the path of the contact surface between the gas initially at rest in the exhaust pipe and the hot exhaust gas flowing out of the engine cylinder. This obviously marks a large discontinuity in temperature levels and hence, values of sonic velocity. The C_+ and C_- characteristics would then be expected to slow down and speed up, respectively, on crossing it. This is quite clearly shown on figure 2. The subsequent P characteristics of course will not mark such large differences in entropy but they will properly account for the entropy variations caused by, for example, the varying strength of a standing shock at the exhaust port. Additionally, it is most interesting in the way that the two P characteristics mark the particle paths and hence illustrate the wave action described by the C_+ and C_- characteristics.

2.5.2 Initial exhaust pulse

It appears from this discussion that the computation is correctly plotting the x-t diagram and it is interesting now to study an example of the more specific kind of information that may be obtained. In particular, figure 3 shows the typical computed pressure wave development in a straight pipe exhaust system for part of the first engine cycle. Here are shown the pressure values behind every C_+ and C_- characteristic in the duct at successive instants of time from E.P.O. to 5.5 milliseconds afterwards. As this calculation required considerably more precision than the previous test case, about 60 C_+ and C_- characteristics were included so that the shape of the pressure waves would be well defined.

The calculated results are remarkably clear in showing certain phenomena. It may easily be seen how the initial wavefront steepens and very nearly forms a shock near the tailpipe outlet. This corresponds with the C_+ characteristics crowding together on the x-t diagram as in figure 2 and has considerable significance in the determination of radiated sound, as shown in the next section.

As the initial positive pulse reaches the tailpipe outlet it is reflected, as expected, as a negative pressure wave. Then, as this reflection moves back upstream, it becomes markedly less steep. This clearly corresponds with the reflected C_- characteristics separating from each other in the expansion wave as, again, shown in figure 2. When the reflected wave reaches the exhaust port, the pressure near the port will be well below the atmospheric value. Such a low pressure wave may be used to improve the scavenging of the combustion products from the cylinder and improve the engine performance. This, then, is part of the exhaust tuning phenomena.

2.6 Radiated Sound

The radiated sound from an engine exhaust system is directly dependent on the velocity values at the tailpipe outlet. These velocity values are obtained from the calculation of the unsteady flow in the pipe by assuming that atmospheric pressure is a boundary condition at the tailpipe end, as explained in section 2.2.

If the tailpipe outlet velocity u(t) is slowly varying, by which is meant that $\left(\frac{du}{dt}\right)_{max} << \Delta u_{max} \cdot \frac{c}{d}$ (i.e., $\omega \cdot \frac{d}{c} << 1$), where d is the tailpipe diameter and c is the speed of sound, then the determination of the far field radiated sound pressure reduces to the consideration of a volume source. It may be shown (for example, Landau and Lifshitz[17] section 73) that the far-field radiated sound pressure for such a simple source in close proximity to the ground is

$$p(t) = \frac{\rho A}{2\pi r_o} \left(\frac{du}{dt}\right)\left(t - \frac{r_o}{c}\right) \qquad (26)$$

where

A = area of tailpipe outlet

r_o = distance from source

ρ, c = atmospheric conditions

In terms of the x-t diagram shown in figure 2, a value of tailpipe outlet velocity is determined each time a C_+ reaches the tailpipe outlet. This velocity value together with the time of the event is stored in an array by the program and at the completion of each computed engine revolution the radiated sound pressure cycle at a particular distance r_o is calculated from the stored values using equation (26).

It is obvious from equation (26) that a rapidly rising pressure wave, caused by C_+ characteristics crowding together, will result in greater radiated noise than would a pressure wave of similar amplitude but less steepness. Hence the importance of pressure wave steepening which occurs in engine exhaust systems, as shown in section 3.

2.7 Slowly Varying Area - Comparison with Known Solution

Ducts of slowly varying area are accommodated in the one-dimensional analysis as shown in section 2.1, and the method used to compute the x-t diagram for a varying area section of a duct is explained in section 2.4. However, as the computation method used several approximations it was considered necessary to check the method by computing a varying area duct problem for which there was a known solution. The case considered was that of an initially weak shock traveling down a duct of decreasing area, for very large changes in duct cross sectional area.

Figure 4 shows the calculated shock Mach number obtained plotted against the diameter of the duct. The theoretically predicted curve in figure 4 was derived from Whitham's theory[16] in which the shock strength is related to the area. This particular theory was found by Whitham to give extremely accurate predictions of the shock strength for the imploding spherical shock (the Guderley problem) for which an exact solution exists. Clearly the calculation method follows very closely the result of Whitham up to a shock Mach number of nearly 2. The reason for the slight discrepancy appearing at Mach 2 is obviously the fact that the computer program approximates all shocks at being weak, as explained in section 2.1. The calculation method is clearly adequate to study engine exhaust systems as shocks in such systems will never have Mach numbers as high as 2.

2.8 Method of Benson

The method of Benson, which is the same method used by Blair, was not adopted for this study as it was believed that it would not be as accurate as the method described above in computing the radiated exhaust noise from an engine, especially when rapidly rising exhaust pulses are present in the exhaust system. Such a rapidly rising exhaust pulse is shown from the measurement presented in section 3 to sometimes result in a pulse of radiated sound pressure of only 10^{-4} seconds duration. Consequently, to adequately follow the associated rapid changes in tailpipe velocity, the use of a basic time step in the calculation of at least less than 10^{-5} seconds is desirable. Now in the case of the method described above in which the paths of C_+, C_- and P characteristics are followed, the necessary small time interval is provided when C_+ characteristics crowd together and change the particle velocity at the tailpipe outlet at very short intervals. Elsewhere in the same calculation, in regions in which the flow is slowly varying, the characteristics will be further apart and less computing effort will be expended, however, this will not at all affect the precision of the radiated exhaust noise calculation as this is determined by the rate of change of the tailpipe velocity (section 2.6). On the other hand, a calculation method, such as that of Benson, which computes the flow at fixed mesh points in the duct, will need quite a large number more mesh points than 60 to resolve the radiated sound pressure cycle as well as the method described above. (Typically 60 C_+ and C_- characteristics were used in the above method.)

To verify the assumption that the method of Benson was not wholly desirable for exhaust noise studies, a comparison was made between a calculation obtained using the program described above, and a similar calculation

performed at Manchester using a standard program based on the analysis of Benson[10]. The calculations were performed to simulate the first exhaust cycle for an engine with a straight pipe exhaust for which steepening of the initial pulse was to be expected. Figure 5 shows the values calculated by the two methods for the pressure at a point in the pipe near the outlet end. Clearly the method of Benson has not adequately described the event although admittedly, only 8 mesh points were used to describe the exhaust system. As mentioned in the introduction, the inclusion of progressively more mesh points in the Benson calculation will improve the pressure trace shown in figure 5, but it is quite reasonable to assume that the method described above will be superior in determining radiated sound pressure.

The accurate way in which other events may be described by the above analysis is shown in the next section.

3. COMPARISON WITH EXPERIMENT

3.1 Experiments

To determine how well the calculation method modeled the events occurring in exhaust systems on operating engines, measurements were taken of various phenomena for three different exhaust systems. These measurements are shown below compared with calculations performed to simulate the same systems. The three exhaust systems tested are shown in figure 6, and include a short straight pipe, a much longer straight pipe and a tuned expansion chamber. The different length straight pipes were used to show the occurrence of pulse steepening in the longer one and the consequently greater radiated sound, whereas, the tuned expansion chamber was used to test the varying area analysis.

The experiments were all performed using a high performance, single cylinder, 125 cc two-stroke motorcycle engine, specifications of which are in Appendix 1. A generator was used to provide constant known loads. Measurements were taken simultaneously of the cylinder pressure cycle (to supply the initial cylinder conditions for the calculation) and the exhaust duct pressure cycle at each of the positions indicated in figure 6 for the three exhaust systems. Then, using the same operating conditions, the far field radiated sound pressure cycle for each system was measured in a free field close to the ground plane. Following section 2.6 the radiation was assumed to be hemispherical.

Both the cylinder and exhaust pipe pressure measurements were obtained using quartz pressure transducers: Kistler type 7031 for the exhaust pipe and type 6005 for the engine cylinder. Each of the transducers was in a water-cooled housing. The resonant frequencies for the transducers in their housings were 10 kHz for type 7031 and 4 kHz for type 6005 (obtained from shock tube measurements), which proved adequate. The radiated sound pressure was measured by a microphone situated 5 m from the exhaust outlet and, considering the distance from the ground plane, destructive interference would have first occurred near 1 kHz. (Ground reflection was considered beyond the scope of the analysis.) Microphones used were a B and K 1/4-inch-type 4136 for the 1.3 m pipe and a 1/2-inch-type 4133 for the others.

For consistency, all pressure measurements taken inside each of the three exhaust systems, and the radiated sound from both the short pipe and the tuned expansion chamber were obtained with the engine operating at 4000 rpm under the same high load. Due to experimental difficulties, the radiated

sound measurement for the 1.3 m pipe was taken with the engine running at 6000 rpm with a low load. Of course, the correct calculation was made for each case.

3.2 Straight Exhaust Pipes

3.2.1 Short pipe

Measurements and calculations for the 0.4 m pipe are shown in figures 7 and 8. The calculations were obtained by running the computer program to simulate several (2) successive engine revolutions, after which a steady state situation was found to be approached. The results shown are then for the second engine revolution.

The computed pressure traces (a) and (c) of figure 7 both show reasonably good agreement, particularly in magnitude, with the measurements. As would then be expected, the computed one-third-octave spectrum, which is simply derived from a Fourier analysis of the trace (c) of figure 7 fairly closely predicts the measured values in figure 8. This measured spectrum was simply obtained by analyzing the recorded sound on a loop of tape using a one-third-octave band filter. Possibly in view of the much closer detailed agreement found for the 1.3 m pipe an for the varying area pipe (discussed below), a main reason for the discrepancies shown in traces (a) and (c) of figure 7 is the fact that the initial region (i.e., in which the flow is far from one-dimensional), which is of the order of two to three diameters from the exhaust port, is a significant fraction (20 - 30 percent) of the 0.4 m pipe length.

Figure 7 shows how the radiated sound pressure cycle is obviously dominated by the large magnitude peak, caused by the initial exhaust pulse.

This is clear from both the measured and calculated cycles (c). Of course, the computed cycle (c) is simply the derivative of the computed tailpipe velocity cycle (b).

3.2.2 Long pipe

Measurements and calculations for the 1.3 m pipe exhaust are shown in figures 9, 10 and 11. In this case, the calculations shown were obtained after three successive engine cycles.

Figure 9 shows that very good agreement is shown for the timing of both the initial and reflected exhaust pulses at all three positions along the pipe, with the magnitudes of these pulses very accurately calculated at the first two positions. On looking at these three measured and calculated traces, the progress of the initial pulse and the subsequent reflections, along the pipe, is quite clear. The initial positive pulse is seen reflected as a negative wave, A, as would be expected, and this is in turn reflected from the then closed exhaust port as another negative wave, marked C.

As similarly indicated previously in figure 3, the calculated pressure cycles at the three positions in figure 9 show the steepening of the initial exhaust pulse as it travels along the pipe. This, of course, corresponds with the C_+ characteristics on the x-t diagram crowding together as in figure 2. This wave steepening is shown more clearly in figure 10 in which the computed information of figure 9 is plotted with a more convenient scale and compared with other measured pressure traces obtained with greater instrument gain. The computed traces in figure 10 show the initial pulse steepening significantly on passing down the pipe and although not identical,

the measured traces also show the steepening of the initial exhaust pulse. In fact, the measurement shows that 1.12 m from the port, a shock wave of low strength has formed.

From the discussion of section 2.6 above, it then follows that the sound pressure radiated by the initial exhaust pulse would be greater for the long pipe than for the short pipe due to the pulse steepening. Results in figures 7 and 11 show this to be the case. Figure 11 shows measured and calculated radiated sound pressure for most of one cycle for a higher engine speed of 6000 rpm, with a lower load. Although the initial pulse in this case would be a little different it is believed that the conclusion is still valid. Therefore, the reason for the much greater peak value is clearly the effect of pulse steepening.

3.3 Tuned Expansion Chamber

The set of results obtained for the tuned expansion chamber, which all related to the same speed and load, are shown in figures 12, 13 and 14. The calculated results were again obtained for the third engine cycle.

In this case, the agreement shown at the measuring positions along the duct, in figure 12, is excellent. Because of the complicated wave reflections it is no longer possible to follow the development of the wave pattern, however, it is clear from traces (3), in particular, that wave steepening does not occur to the same degree as in the case of the long straight pipe. This results as the initial pulse is partly reflected at the increasing area section and so is diminished in strength. As a consequence of this, the radiated sound pressure peak resulting from the initial pulse, as shown in figure 13, is now of much lower amplitude than in the case of the long pipe.

Figure 13, in fact, shows clearly that the calculated radiated sound pressure peak closely simulates the measured peak in both magnitude and duration, even though its duration is barely 10^{-4} seconds.

The computed and measured one-third-octave spectra also show very good agreement in figure 14, as would be expected from the agreement of figure 13. There is a noticeable error only in a region near 1 kHz. This, in fact, is the region where the first occurrence of destructive interference from ground reflection would be expected (see section 3.1 above).

3.4 Discussion

The very good results shown for the case of the tuned expansion chamber above indicate that the modeling of slowly varying area ducts is as accurate as the basic method that describes straight pipes. In fact, the correspondence of some of the values, in particular, the pressure cycles at positions (1), (2) and (3) in figure 12, and the radiated noise spectrum of figure 14, is remarkable. Again, as for the straight pipes, the precise prediction of the magnitude and duration of the very short peak in the radiated sound pressure cycle shows the benefit of computing the x-t diagram in the manner described above. Once more, the value of a small time interval and close determination of the velocity values at the tailpipe outlet is clear. It is then expected that any straight or gradually varying area duct may be studied with the same accuracy.

By following the development of the initial pulse along both the long straight pipe and the tuned expansion chamber in figures 10 and 12, it is clear that the effects of wave steepening and pulse reflection will result in a large variation in the radiated sound pressure peaks for the long pipe,

the shorter pipe and the tuned expansion chamber. This is clear from figures 7, 11 and 13, where the measured radiated peak values are 12 Pa for the short pipe, 22 Pa for the long pipe and 6 Pa for the tuned expansion chamber. For each case, it is clear that the radiated sound pressure cycle is dominated by this large magnitude peak caused by the initial pulse. This large peak obviously affects the peak sound pressure level, whereas, the lower magnitude fluctuations will significantly affect the rms level.

Finally, some comment needs to be made of the poorer agreement obtained for the pressure cycles nearest the end of the two long exhaust systems. These are trace (c) in figure 9 for the 1.3 m straight pipe and trace (4) in figure 12 for the tuned expansion chamber. It appears most likely that the omission from the analysis of neat loss to the pipe walls is the largest source of error, as the exhaust gas temperature does decrease slightly along an exhaust system of about 1.3 m length used on a small engine. The errors caused by this omission are clearly not significant in the general calculation of the wave phenomena as shown by the otherwise very good results. However, it should be realized that the duct wall pressure near the open tailpipe end is formed by the summation of an incident pulse and its reflection of opposite sign arriving a very short time later. There is then an accentuated error in this pressure trace which does not imply that large errors exist in the general calculation.

4. CONCLUSIONS

The use of the method of characteristics, by computing the x-t diagram in the way described, has been shown to be a highly satisfactory means for studying radiated noise for two-stroke engine exhaust systems. The method

is obviously suitable for four-stroke engines. The method has successfully been used to accurately model both the development of the initial exhaust pulse in an exhaust system and the spectrum of the sound radiated. Of particular merit is the way the method closely follows both wave steepening and the resultant rapid changes in velocity at the tailpipe outlet. Straight pipes of different length and slowly varying area ducts have both been considered.

It is expected that the method could be readily extended to include many exhaust system elements, such as a step change in cross section and a simple constriction, for which the one-dimensional approximation is still applicable. In such cases an account of entropy increases in the flow at discontinuities may be included and hence the backpressure of these devices may be known. The method could conceivably be extended to branched systems and hence many muffler systems, such as side branch filters could be analyzed and multi-cylinder engines could be studied.

This method of full nonlinear variable entropy analysis clearly has advantages over the simple lumped element theory and is an improvement on the distributed impedance model for two reasons. Firstly, wave steepening is correctly allowed for and, secondly, the precise sound source impedance is included. Consideration has also been given to the similar previous uses of the method of characteristics and to studies made using finite difference methods which have been regarded as less suitable for radiated noise studies. The method described was developed to provide the necessary fine resolution of events at the tailpipe outlet to accurately determine radiated exhaust noise.

APPENDIX 1

Motorcycle Engine Specifications

The engine used is from a Suzuki TS 125 model motorcycle. The engine is a single cylinder air-cooled two-stroke type, is crankcase scavenged and has piston operated ports.

Basic Dimensions

compression ratio	6.7:1
bore X stroke	56 x 50 mm (2.20 x 1.97 in)
swept volume	123 cc (7.5 in^3)
crankcase compression ratio	1.3:1
maximum power	9.7 kW (13 hp) at 7000 rpm
maximum torque	13.3 N·m (9.8 lbf-ft) at 6500 rpm
ignition timing	21 - 23° BTDC

Port Timing

inlet	open 70° BTDC	close 70° ATDC
exhaust	open 98° ATDC	close 98° BTDC
transfer	open 116° ATDC	close 116° BTDC

Total Area of Fully Open Ports

exhaust	4.032×10^{-4} m^2
transfer	6.16×10^{-4} m^2

REFERENCES

1. Davis, D. D.; Stokes, G. M.; Moore, D.; and Stevens, G. L.: Theoretical and Experimental Investigation of Mufflers with Comments on Engine-Exhaust Muffler Design. NACA Report 1192, 1954.
2. Alfredson, R. J.; and Davies, P. O. A. L.: The Radiation of Sound from an Engine Exhaust. J. Sound and Vibration 13 (4), 1970, pp. 389-408.
3. Alfredson, R. J.; and Davies, P. O. A. L.: Performance of Exhaust Silencer Components. J. Sound and Vibration 15(2), 1971, pp. 175-196.
4. Young, C.-IJ.; and Crocker, M. J.: Acoustical Analysis, Testing, and Design of Flow-Reversing Muffler Chambers. J. Acoustical Society of America 60(5), 1976, pp. 1111-1118.
5. Young, C.-IJ.; and Crocker, M. J.: Finite Element Acoustical Analysis of Complex Muffler Systems With and Without Wall Vibrations. Noise Control Engineering 9(2), 1977, pp. 86-93.
6. Jones, A. D.: Noise Characteristics and Exhaust Process Gas Dynamics of a Small 2-Stroke Engine. PhD Thesis. U. of Adelaide. 1978.
7. Coates, S. W.; and Blair, G. P.: Further Studies of Noise Characteristics of Internal Combustion Engine Exhaust Systems. SAE Paper 740713, 1974.
8. Blair, G. P.: Computer-Aided Design of Small Two-Stroke Engines for Both Performance Characteristics and Noise Levels. C120/78, I. Mech. E. Conference Publications 1978-5, 1978.
9. Benson, R. S.; Garg, R. D.; and Woollatt, D.: A Numerical Solution of Unsteady Flow Problems. Int. J. Mech. Sci. 6, 1964, pp. 117-144.

10. Anon.: Computer Program to Simulate a Crankcase Compression Spark Ignition Engine. Users Manual for Data Preparation. Mark II (with receivers) Vols. 1 and 2. The U. of Manchester Institute of Science and Technology. 1977.

11. Blair, G. P.; and Johnston, M. B.: Unsteady Flow Effects in Exhaust Systems of Naturally Aspirated, Crankcase Compression Two-Cycle Internal Combustion Engines. SAE Paper 680594, 1968.

12. Karnopp, D. C.; Dwyer, H. A.; and Margolis, D. L.: Computer Prediction of Power and Noise for 2-Stroke Engines with Power Tuned, Silenced Exhausts. SAE Paper 750708, 1975.

13. Lakshminarayanan, P. A.; Janakiraman, P. A.; Gajendra Babu, M. K.; and Murthy, B. S.: Prediction of Gas Exchange Processes in a Single Cylinder Internal Combustion Engine. SAE Paper 790359, 1979.

14. Walter, G. A.; and Chapman, M.: Numerical Simulation of the Exhaust Flow From a Single Cylinder of a Two-Cycle Engine. SAE Paper 790243, 1979.

15. Rudinger, G.: Wave Diagrams for Non-Steady Flow in Ducts. (D. Van Nostrand), 1955.

16. Whitham, G. B.: Linear and Non-Linear Waves. (J. Wiley), 1974.

17. Landau, L. D.; and Lifshitz, E. M.: Fluid Mechanics. (Pergamon), 1959.

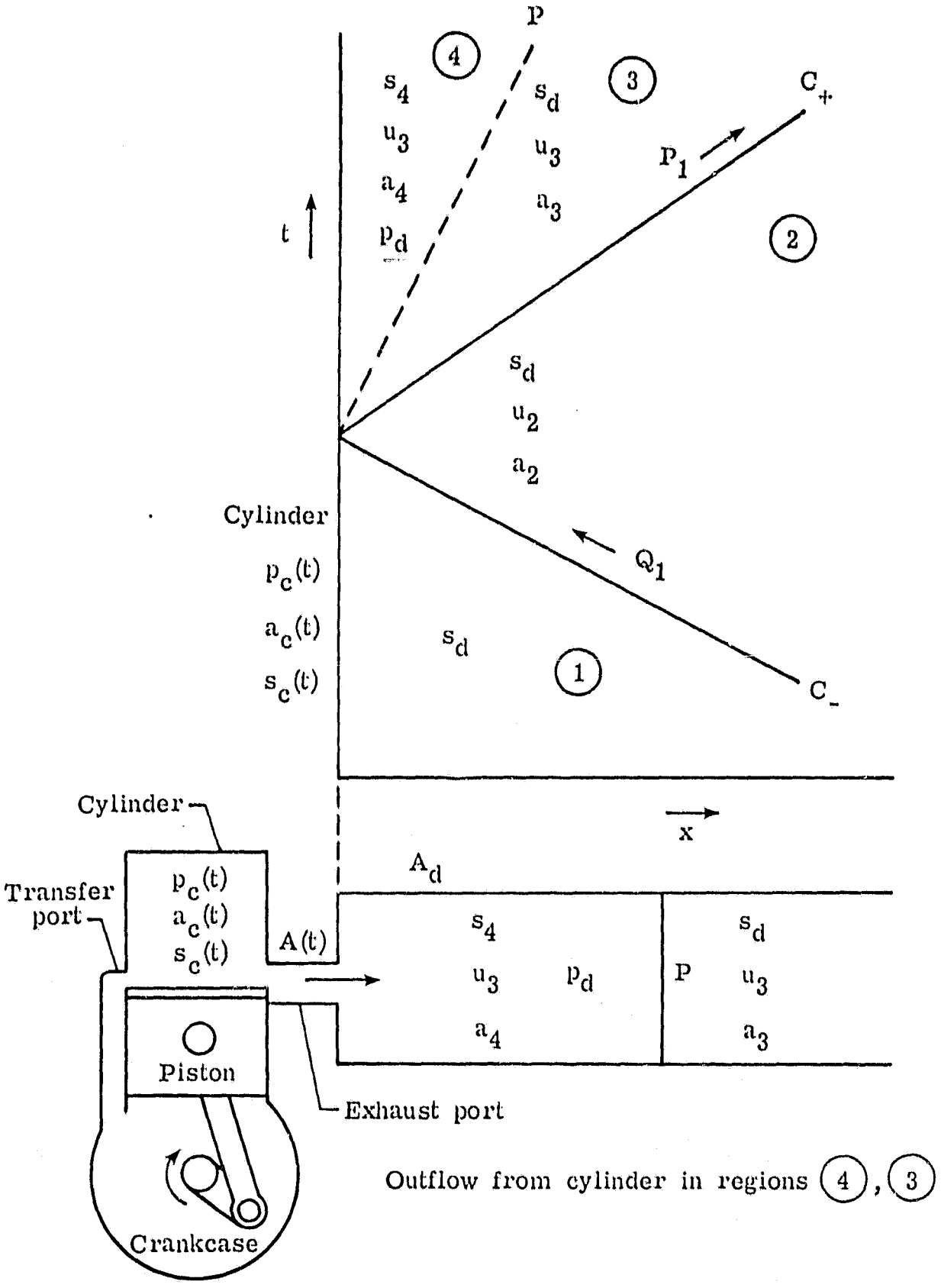

Figure 1.- C_- characteristic causing outflow from cylinder.

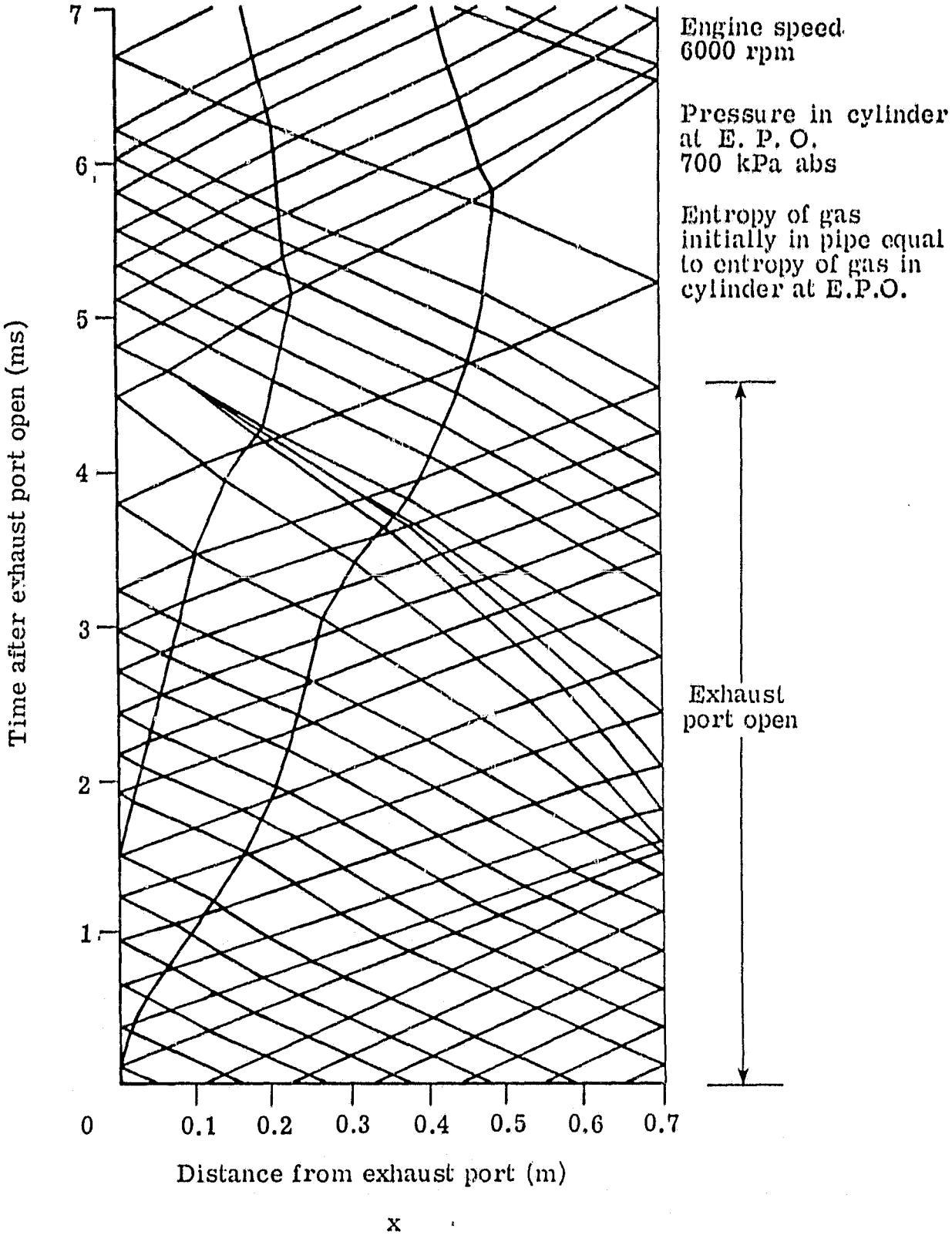

Figure 2.- Computed x-t diagram for engine with 0.7 m straight pipe exhaust.

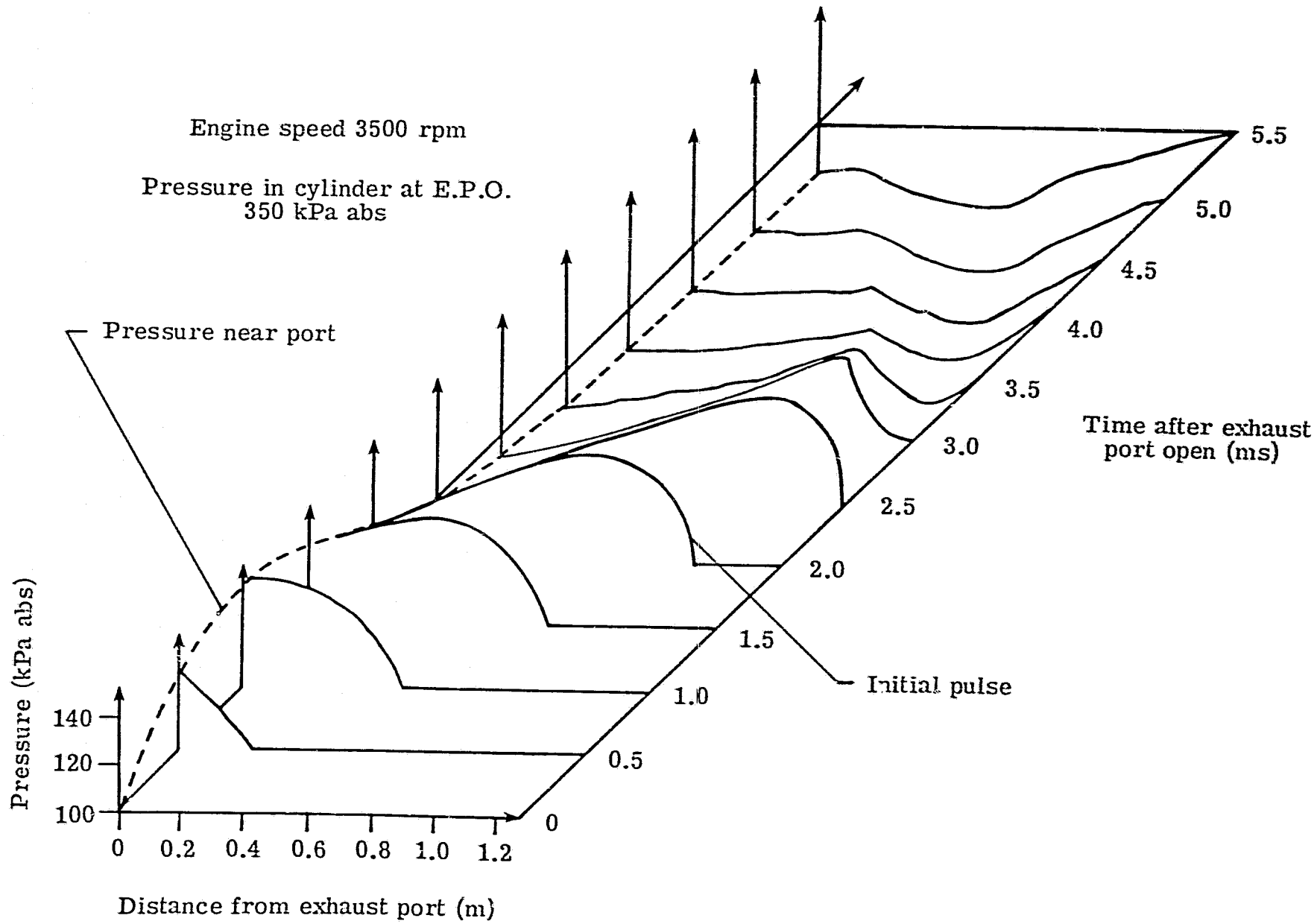

Figure 3.- Computed pressure wave development in 1.3 m straight pipe exhaust.

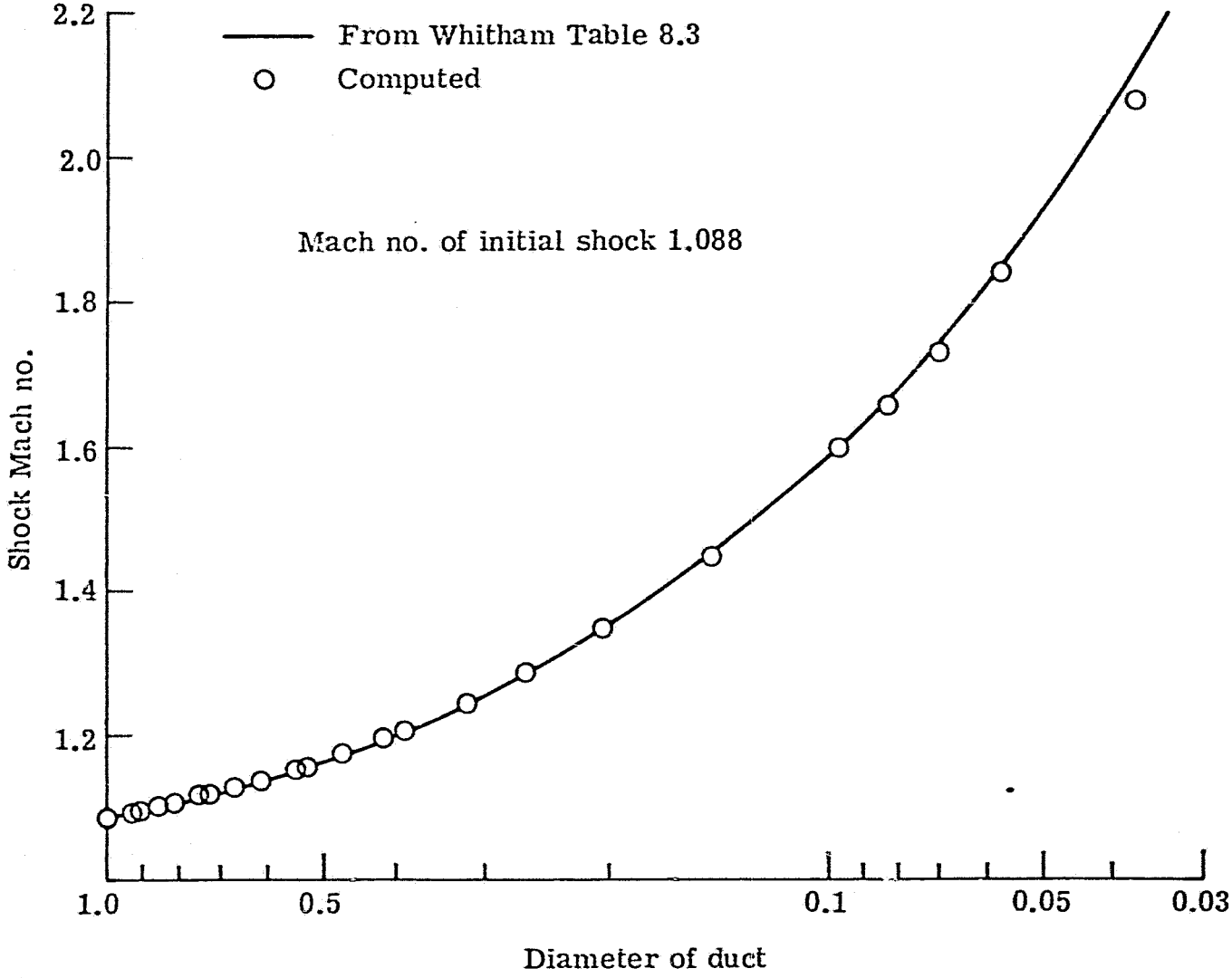

Figure 4.- Shock propagation along duct of decreasing diameter.

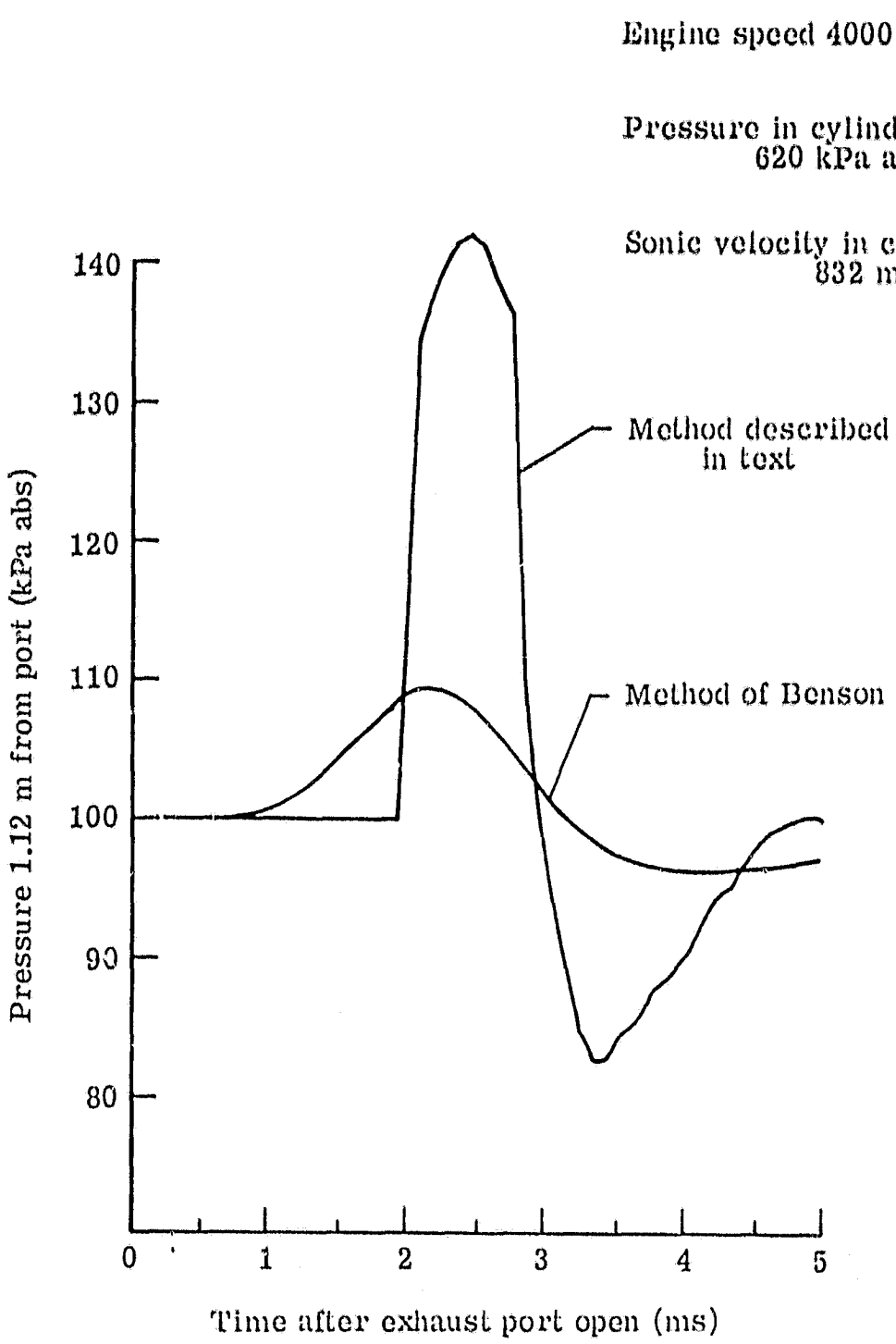

Figure 5.- Computed pressure waves in 1.3 m straight pipe exhaust.

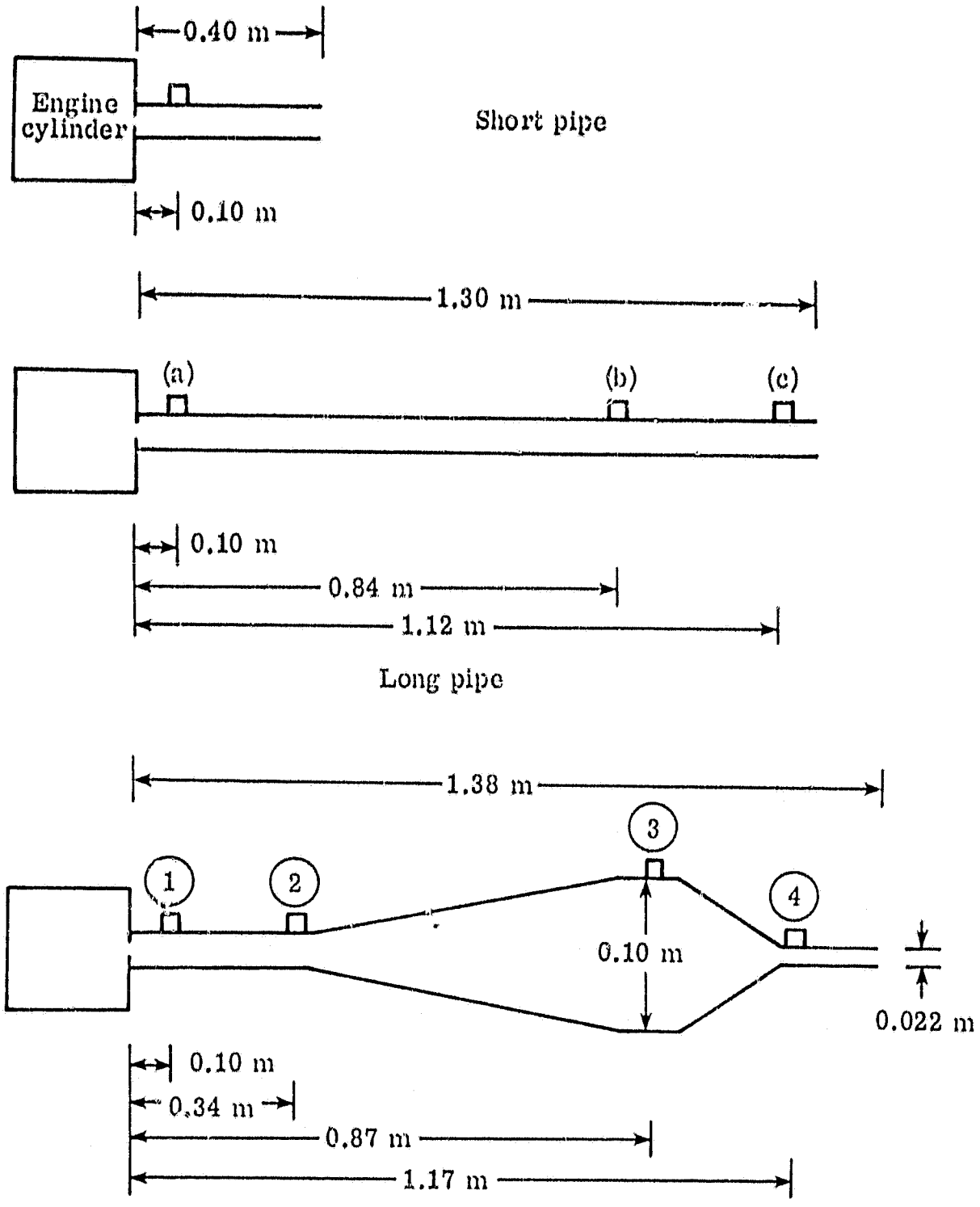

Short pipe, long pipe, first section of tuned expansion chamber all of diameter 0.04 m.

Figure 6.- Experimental exhaust systems showing measuring positions.

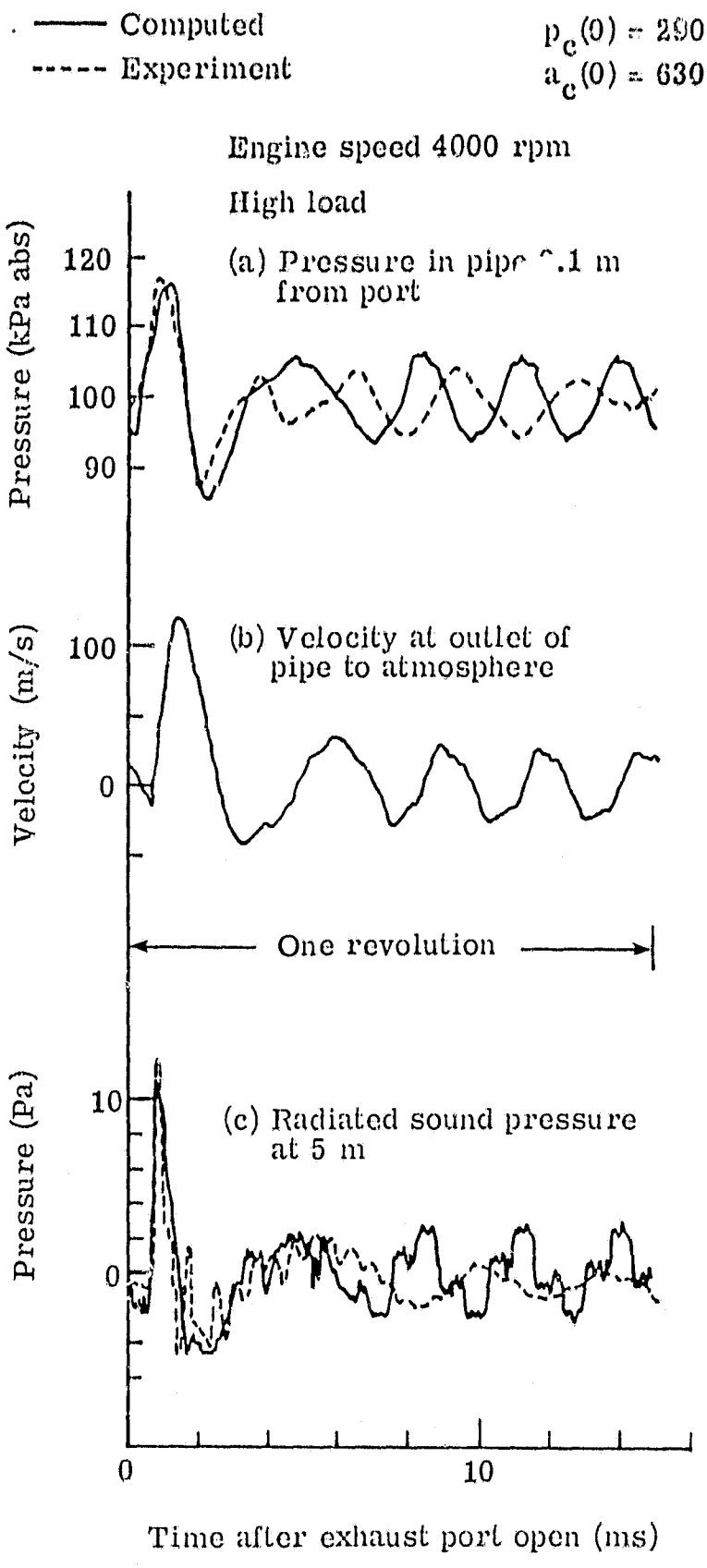

Figure 7.- Calculations and measurements for 0.4 m straight pipe exhaust.

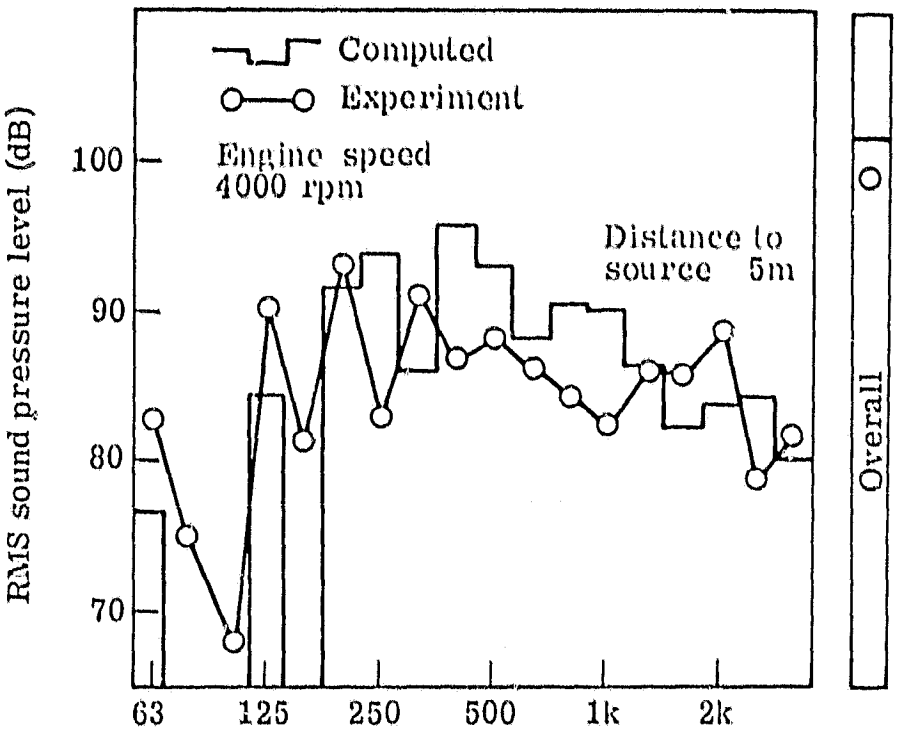

Figure 8.- Third-octave radiated noise from 0.4 m straight pipe exhaust.

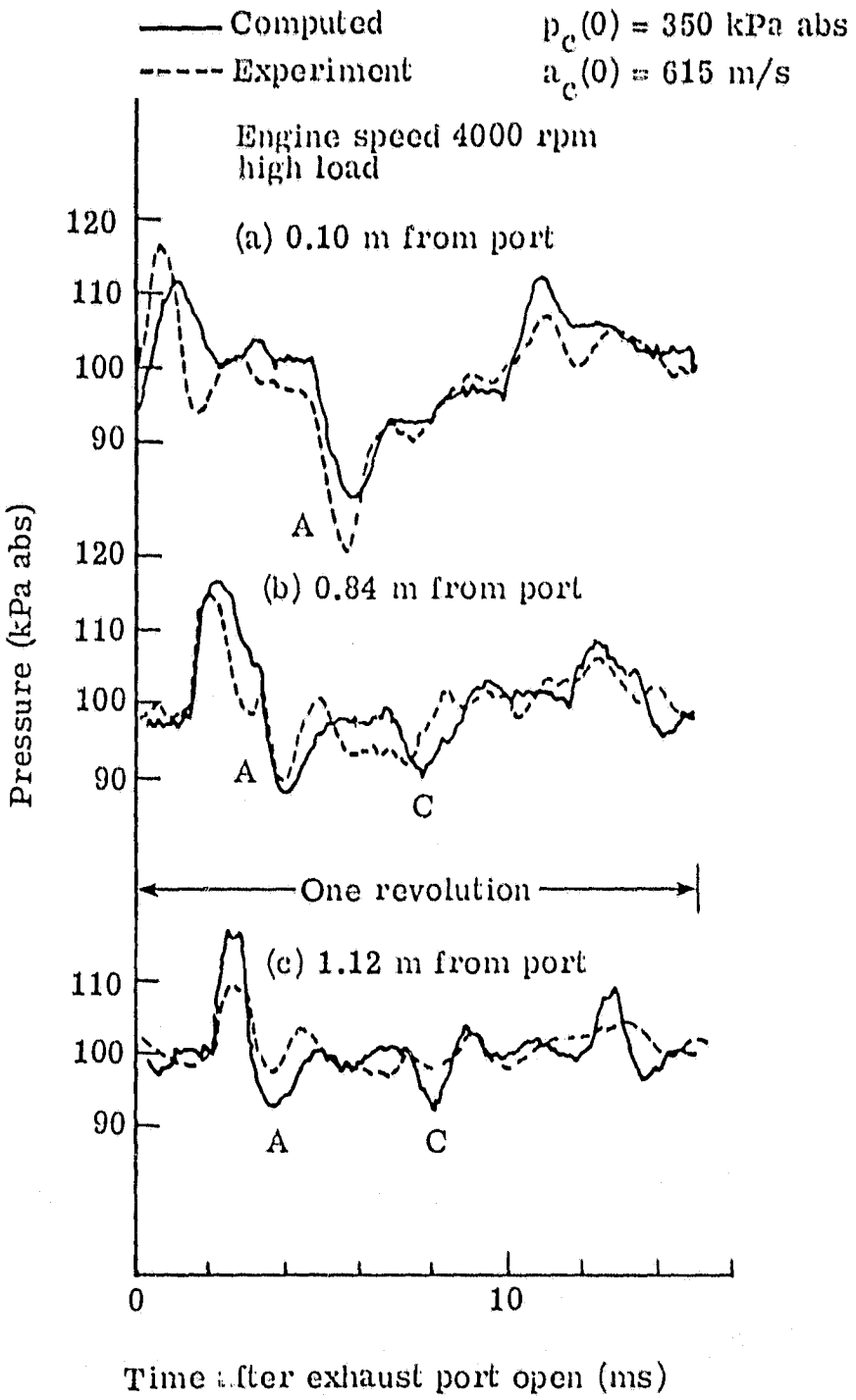

Figure 9.- Pressure waves in 1.3 m straight pipe exhaust.

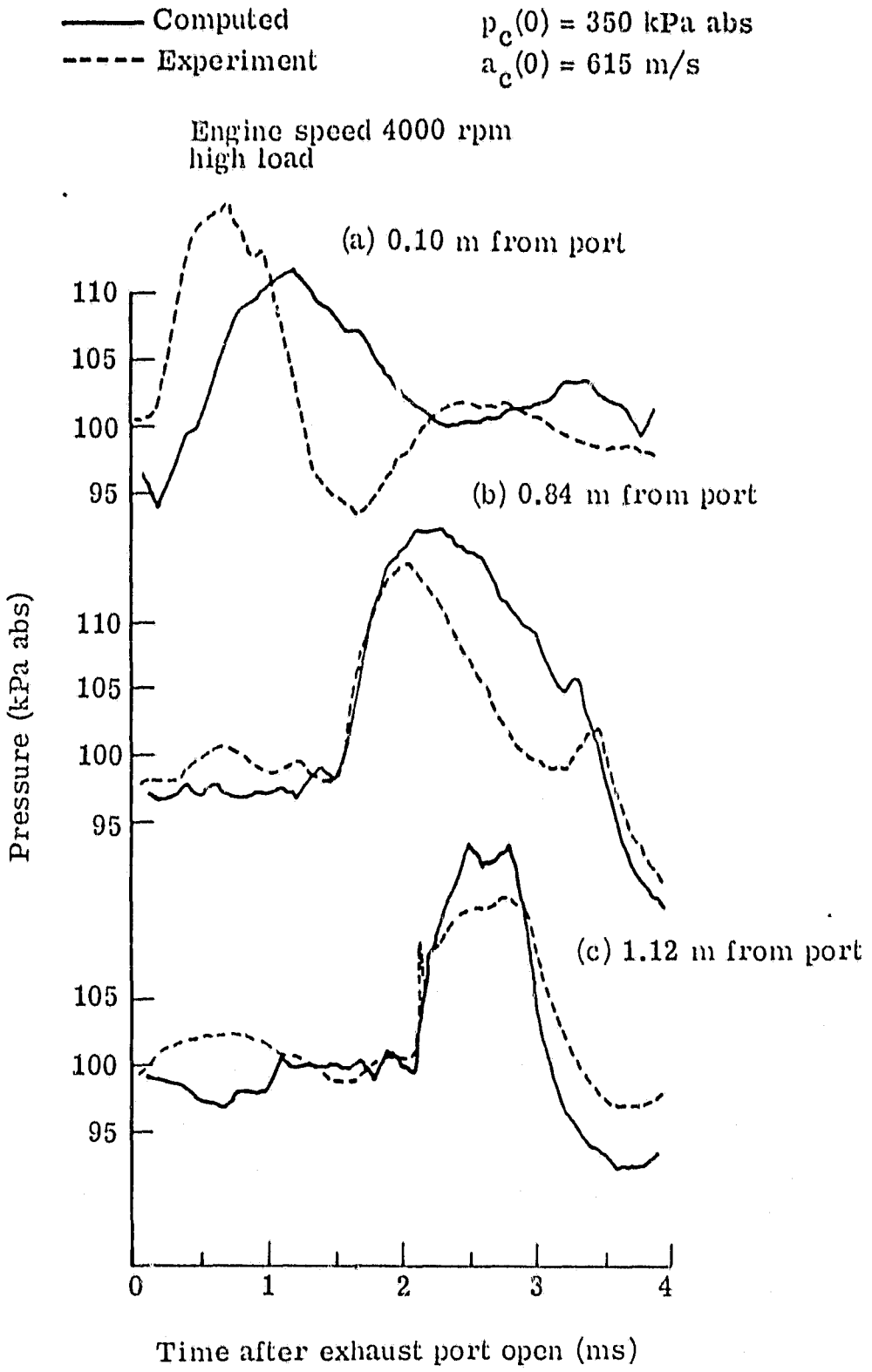

Figure 10.- Initial pulse steepening in 1.3 m straight pipe exhaust.

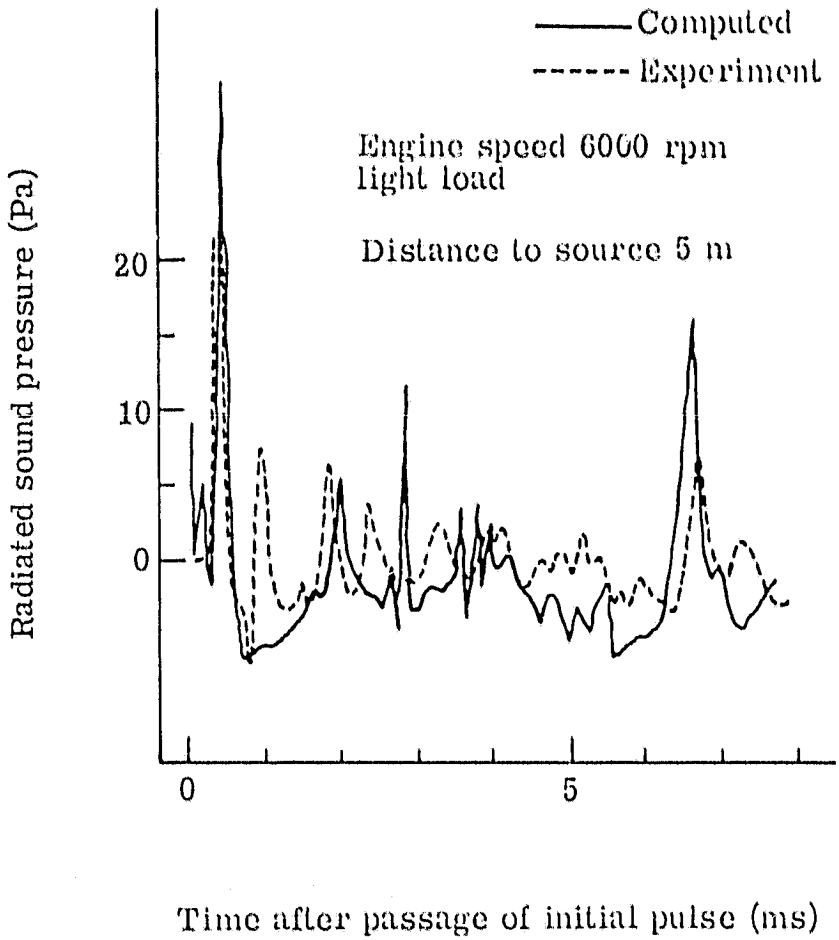

Figure 11.- Sound pressure radiated from 1.3 m straight pipe exhaust.

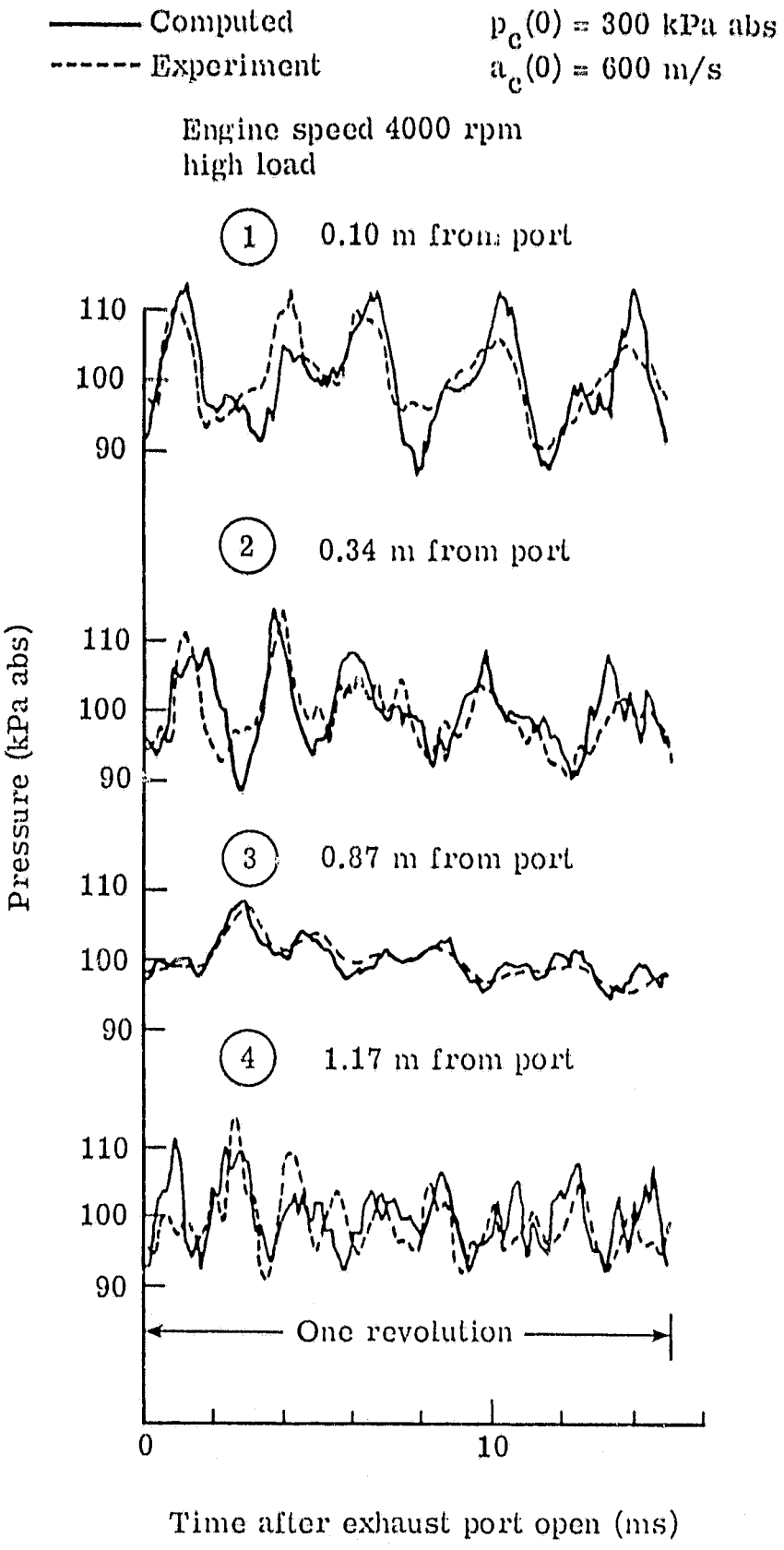

Figure 12.- Pressure waves in tuned expansion chamber.

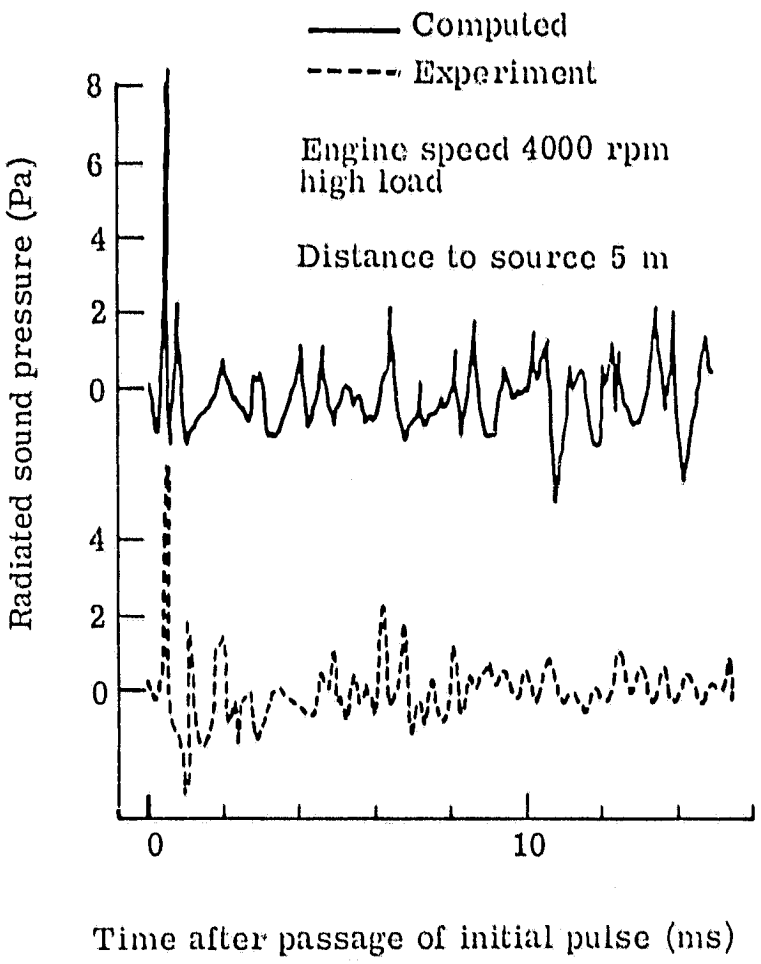

Figure 13.- Sound pressure cycle radiated from tuned expansion chamber.

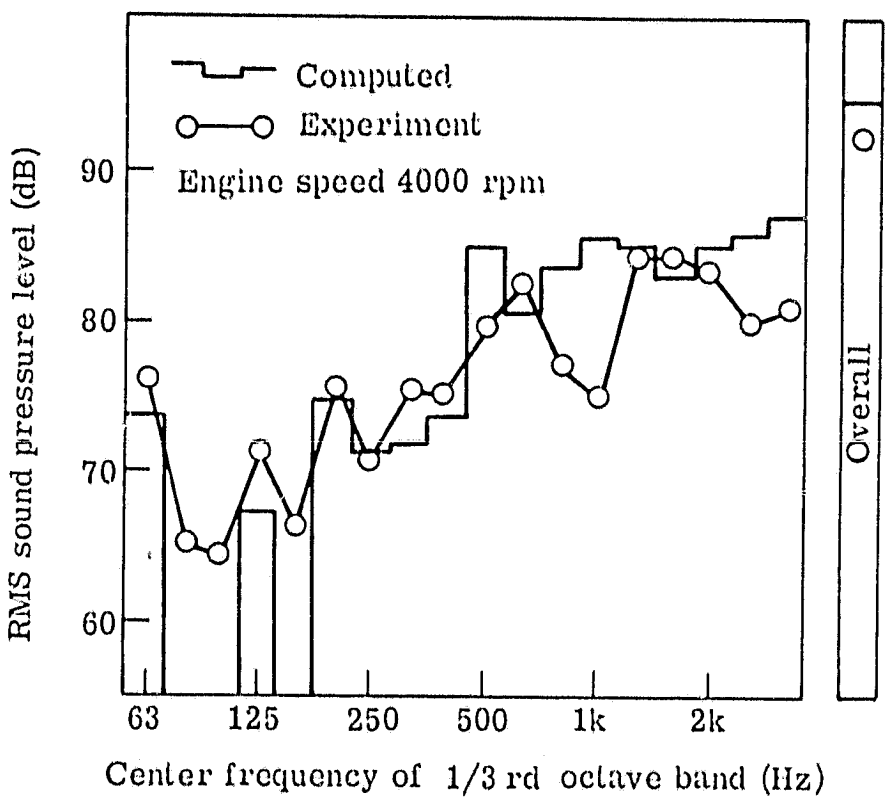

Figure 14.- Third-octave radiated noise from tuned expansion chamber.